General Disclaimer

One or more of the Following Statements may affect this Document

- This document has been reproduced from the best copy furnished by the organizational source. It is being released in the interest of making available as much information as possible.

- This document may contain data, which exceeds the sheet parameters. It was furnished in this condition by the organizational source and is the best copy available.

- This document may contain tone-on-tone or color graphs, charts and/or pictures, which have been reproduced in black and white.

- This document is paginated as submitted by the original source.

- Portions of this document are not fully legible due to the historical nature of some of the material. However, it is the best reproduction available from the original submission.

Produced by the NASA Center for Aerospace Information (CASI)

INFRA-RED and
ELECTRO-OPTICS
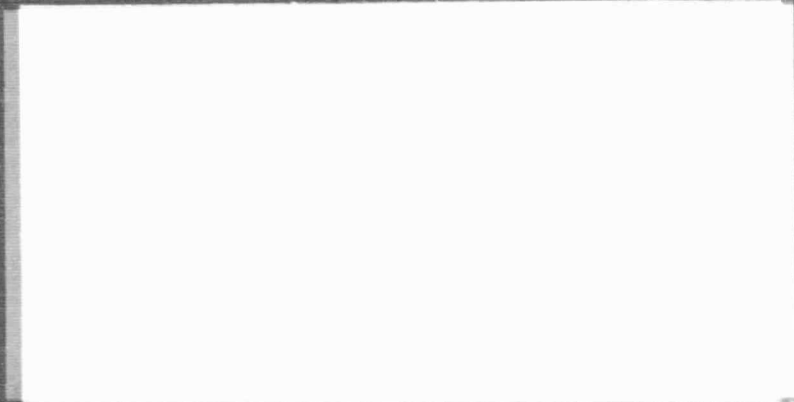
development   components

research   systems

manufacture   instruments

BARNES ENGINEERING COMPANY
30 Commerce Road   Stamford, Connecticut

BEC PROJECT 3744
TR 3744-IB

BARNES ENGINEERING COMPANY
30 Commerce Road
Stamford, Connecticut

PHASE IB REPORT

Design of
Field Switched Edge Tracking
Earth/Lunar Horizon Sensor System

PREPARED BY:

Frank Schwarz
Frank Schwarz

Thomas Falk
Thomas Falk

Peter E. Spangenberg
Peter E. Spangenberg

APPROVED BY:

Robert W. Astheimer
Robert W. Astheimer
Technical Director
DEFENSE AND SPACE DIVISION

DATE: March 8, 1966

TABLE OF CONTENTS

LIST OF ILLUSTRATIONS

LIST OF TABLES

1. INTRODUCTION

The Earth/Lunar Horizon Sensor System development program began with a study phase. In this study phase, a great variety of different infrared horizon sensor approaches were investigated with a view to determining which system promised to meet the stringent requirements of high accuracy for both earth and lunar missions (determination of local vertical to 0.1°), and which had a reliability figure far superior to that of any presently existing sensor system.

The trade-off study was completed some time ago and resulted in several study reports. We have now entered into the design phase of the program, which began with a 2-month period of detail sensor design limited to the one chosen system-- an edge tracker employing the technique of "field switching" in which a field of view at the edge of the planet is compared with an equal field which views a region in space serving as the reference signal. It was only in recent weeks that we have come to the conclusion that this system can best be implemented through use of thermopile detectors which permits free choice of the separation of the two fields of view. This results in

a simple optical system design and eliminates the need for an optical chopper, and thus brings about a reduction in size, weight, and power and greatly increases the system reliability.

This report describes the basic design of the chosen Earth/Lunar Horizon Sensor System, giving some detail of circuit design and performance where such information is available. Rather than to formally separate a formal design study (Phase IB) from the hardware phase of the program, we have chosen to pursue both phases in parallel in order to expedite completion of the engineering model and to make up for some lost time in the trade-off study (Phase IA) caused by a review of the problem of increasing the horizon sensor's speed of response if this should prove to be desirable. We have therefore proceeded both with the paper design and certain phases of breadboarding and hardware work and have ordered some of the longer lead-time items. Some of the circuits (e.g., the servo drive, tachometer circuitry, preamplifier, etc.) have been designed, breadboarded, and tested.

Therefore, despite the loss in time referred to earlier, we hope to continue the hardware work and increase

its pace and thus complete the engineering model in accordance with the original schedule. We believe, further, that the system we are currently designing will be capable of achieving the desired accuracy and that it will be compact and rugged and will exceed the reliability figures quoted in our Phase IA Report. The system presently being designed is versatile and is believed to have good growth potential.

In the sections which follow we will discuss the optical and mechanical design, the electronic circuitry, and the expected performance characteristics.

2. MECHANICAL/OPTICAL DESIGN

As pointed out in the Introduction, this report dis-
cusses the design of a "Field Switched" Edge Tracking Horizon
Sensor using thermopile detectors. In carrying out this design,
several approaches utilizing thermopile switching have been
considered and evaluated. The following is a description of
the chosen design configuration, shown in Figure 2-1, and a
discussion of the factors which led to this decision.

The chosen system, as is seen from Figure 2-1, uses
an optical telescope module including a detector and aspheric
lens which is pivoted by a torquer to provide it with both
search and tracking capability.

Two methods of scan acquisition have been considered.
The first method consists of a fixed optical telescope assembly
designed to accept incoming collimated radiation to the two
thermopile detectors. A pivoted flat mirror is placed immediately
in front of the objective as shown below. The servo components,

Acquisition range
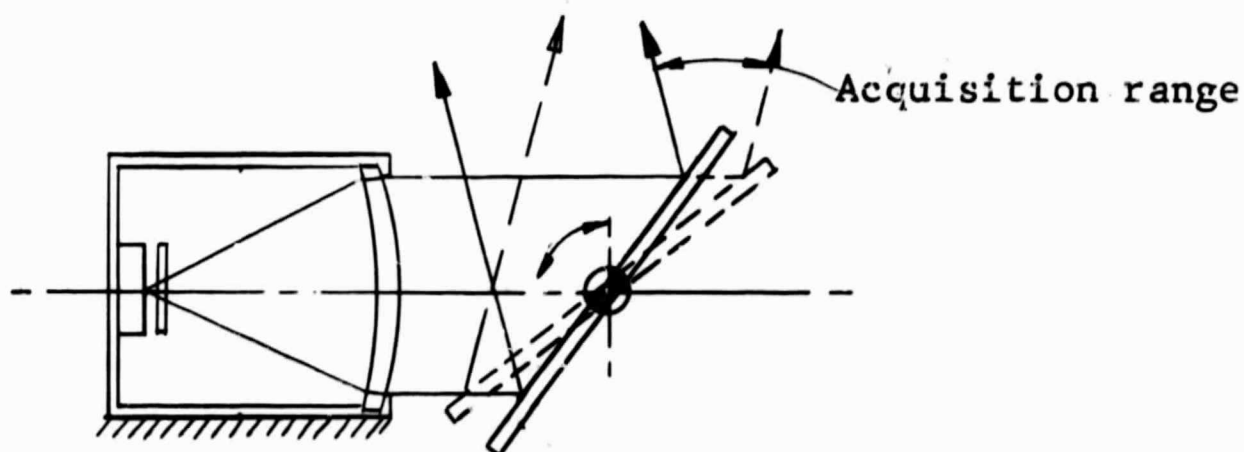
Figure 2-2
Fixed Telescope with Pivoting Mirror

LEAD WIRES

AEROFLEX BRUSHLESS
TACHOMETER TG18W-125

SIGNAL PROCESSING
P.C. BOARDS

CONNECTOR

4 DIA

10°   1°

AEROFLEX BRUSHLESS
TORQUER TG18W

OFFSET RADIATION
SOURCE

SUN FIELDS
SUPERIMPOSED
WITH MAIN FIELD

WEDGE
ELEMENT

ASPHERIC
SILICON
LENS WITH
A.R. COAT-
ING

SIZE 25
"PANCAKE"
SYNCHRO

SILICON FILTER SUBSTRATE

THERMOPILE DETECTORS

7 1/2

THERMOPILE PREAMPLIFIER
P.C. BOARD

SILICON SUN DETECTORS

TRANSISTOR DRIVE SWITCHES
FOR TORQUER AND OUTPUT
PROCESSING P.C. BOARD

FIGURE 2-1
CONCEPTUAL LAYOUT
THERMOPILE HORIZON
EDGE TRACKER
2/15/66   PROJECT 3744
REV A   6/11/66
REV B - 3/14/66

consisting of a torquer, tachometer, and position readout, are coupled directly to the mirror. The second method eliminates the flat mirror and pivots the telescope and servo components directly as shown in Figure 2-1. The first method has the advantage of a smaller moment of inertia and weight of the pivoted assembly, which will result in a slight decrease in the servo loop error. A second advantage is that flexing wires will not be required for electrical connection to the detector/preamplifier assembly. However, there are four disadvantages which make this system less desirable than the latter:

(1) The acquisition range is limited unless the flat mirror is made excessively large. A mirror of approximately 2 x 5-1/2 inches would be required to achieve a ±30° range with a 2-inch diameter aperture optical system. A 2 x 4 inch mirror is required for ±15°.

(2) The overall size of the sensor head will be larger in order to accommodate the pivoted mirror.

(3) The angular resolution requirement of the shaft encoder is twice as severe because a 1° rotation of the mirror displaces the optical axis by twice the angle.

2 - 4

(4) The possibility of aperture chopping exists on
the surface of the mirror. With a large (20°) field switching
angle, incoming radiation from space and the planet will be
reflected from two different portions of the mirror. These
mirror areas are overlapped to a large extent; however, the
portions that are not common to both switching positions will
present an additional radiance source to each of the detectors.
If the emissivity of the mirror is uniform over the entire sur-
face and there are no temperature gradients, this will not
present a problem. However, a degradation of the mirror re-
flectance in a critical area by only a few percent will produce
a detector signal close to that which will be produced by a 90°K
lunar target. This problem does not exist with the second
method because the optical path of radiation to both thermopile
detectors is identical.

For these reasons, the method of pivoting the tele-
scope has been selected for this application. The angular
moment of inertia for the pivoting telescope system is approxi-
mately 20% greater and its effect on the servo loop accuracy
is considered to be insignificant. In some respects, a large

moment of inertia can be considered as an asset. With the
system tracking a horizon edge, an attitude perturbation
(acceleration) of the vehicle will cause the case of the sensor
to be angularly displaced, but because of the inertia force,
the telescope assembly will tend to remain pointed on the horizon
edge. The required power for the torquer would therefore be
reduced during the tracking mode. On the other hand, the power
and/or time required for initial horizon edge acquisitions will
be greater.

Several optical systems have been considered for the
telescope section. Two systems in particular appear to satisfy
the optical gain requirements and may readily be incorporated
in the design. The first system is essentially a Schmidt tele-
scope consisting of a silicon corrector plate and a spherical
reflector as shown below. The corrector plate is coated with
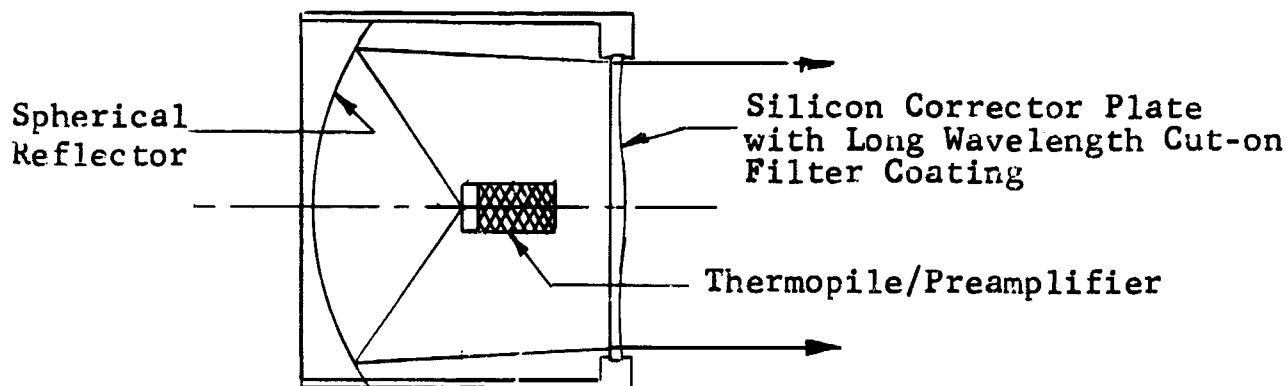a long wavelength cut-on filter.

Spherical Reflector

Silicon Corrector Plate
with Long Wavelength Cut-on
Filter Coating

Thermopile/Preamplifier

Figure 2-3
Schmidt Telescope with Silicon Corrector Plate

2 - 6

The second system, which has several advantages and has been selected for the program, consists of an aspheric silicon lens. A thin (1 mm) filter substrate will be placed immediately in front of the detector to reject the short wavelengths. The lens will be anti-reflection coated to maximize transmission.

A comparison of the two systems is made and tabulated in Table 2-1 to illustrate the type of design trade-offs that must be made before the optimum system can be chosen. In both systems, preliminary ray traces have been made, which indicate that optical aberrations can be controlled to an acceptable level. The design of the remaining portions of the edge tracker will not be appreciably affected by the optical barrel design. The items marked with an asterisk (*) in Table 2-1 are felt to be advantageous to the indicated system. Unmarked items are either essentially equal in advantage or have no significance in themselves and are included mainly for information purposes.

The selection of the aspheric lens system, although resulting in approximately 20% lower sensitivity, is based primarily on considerations of ease in development, fabrication,

TABLE 2-1 Comparison of Schmidt and Aspheric Lens Optical Systems for Thermopile Detector Horizon Edge Tracking System

Design Parameter	Schmidt	Aspheric Lens
(1) Number of Refractive Elements	*1 (2 mm total thickness)	2 (4 mm total thickness)
(2) System Focal Length	1 inch	2 inches
(3) Aperture Diameter	2 inches	2 inches (may be readily increased)
(4) F/Number	0.5	1
(5) Detector Size - mm	1.27 x 4.5	1.27 x 9.0
(6) Field of View - degrees	2.87 x 10	1.44 x 10
(7) Spectral Transmission Efficiency	~40%	~28%
(8) Obscuration Losses	~20% (preamplifier obstruction)	~2% (sun detector obstruction)
(9) Effective Transmission Efficiency	*~32%	~27.5%
(10) Sensitivity with 90°K Moon	*3.6 µvolts/0.2°	3.1 µvolts/0.2°
(11) Output on 90°K Moon with Field of View Filled	51.5 µvolts	22 µvolts
(12) Relative Cost of Optics	1.4	*1

TABLE 2-1 (cont.)

Design Parameter	Schmidt	Aspheric Lens
(13) Focusing Sensitivity	0.003 inch/0.1°	*0.009 inch/0.1°
(14) Preamplifier Packaging and Maintainability	Special cordwood encapsulated package.	*Conventional printed circuit board construction.
(15) Available Space for Preamplifier	Must be minimized to prevent optical obscuration. See Item (9).	*Adequate - no obscuration problem.
(16) Evacuation Technique	Entire optical telescope must be sealed and evacuated.	*Thermopile detector will be enclosed with the filter substrate and evacuated.
(17) Sun Detectors - silicon	Will be mounted on axis close to the corrector plate. Sun energy will enter through a small glass aperture (pinhole). Alignment will be difficult.	*Will be mounted off axis adjacent to thermopiles. Sun energy will enter through a small glass wedge aperture. Because of the greater distance and accessibility, alignment will be readily accomplished.
(18) Moment of Inertia of Optical Barrel	4.5 x 10⁻⁴ lb-in sec²	5.5 x 10⁻⁴ lb-in sec²
(19) Offset Heater	Located outside of telescope section.	*Located inside telescope section.

and alignment. If necessary, the sensitivity may be increased by simply increasing the entrance aperture. For a given field of view, regardless of focal length, sensitivity increases with the square of the aperture diameter. An aperture increase is more readily accomplished with the aspheric lens system than with a Schmidt system.

It is intended that the servo components be of the form illustrated in Figure 2-1. In order to minimize the number of bearings required and eliminate the need for couplings, each of the components (i.e., torquer, tachometer, and shaft position readout) will be of the hollow shaft "pancake" type. One pair of dry lubricated bearings of special construction to minimize static friction will be required.

The size of the sensor head will be approximately as indicated in Figure 2-1. However, a conservative approach was taken on this initial design layout and a substantial size reduction is feasible. For example, the entrance aperture is scaled to a 2-1/2 inch diameter. In all probability, a 2-inch aperture will be sufficient which will result in a 1/2 inch reduction in both length and diameter. If two or more heads are combined into one assembly there will be a further reduction

in total unit volume and weight. Final definition will be
made after the mechanical interface requirements have been
established.

3. ELECTRONICS DESIGN

3.1 Servo Operation

To track the planetary horizon, a d.c. torquer will rotate the optical barrel. The design for the electronic driving circuits has been conceived, with emphasis on power economy and servo stability for a wide range of planetary radiant intensities. The torquer-drive block diagram is given in Figure 3-1.

Each end of the torquer winding can be connected by means of transistor single-pole, double-throw switches to either ground or B^+. Thus, depending on the position of the switches, the torquer drives clockwise, counterclockwise, or not at all (if both ends are connected to ground or both ends to B^+). The amount of torque developed in either direction will be controlled by means of pulse width modulated driving circuits. Two variable pulse width monostable multivibrators control the state of the two single-pole, double-throw switches. (One multi to each SPDT switch.) Both multivibrators will be triggered by sharp pulses of constant repetition rate (about 1000 pps) derived from the inverter power supply of the edge tracker.
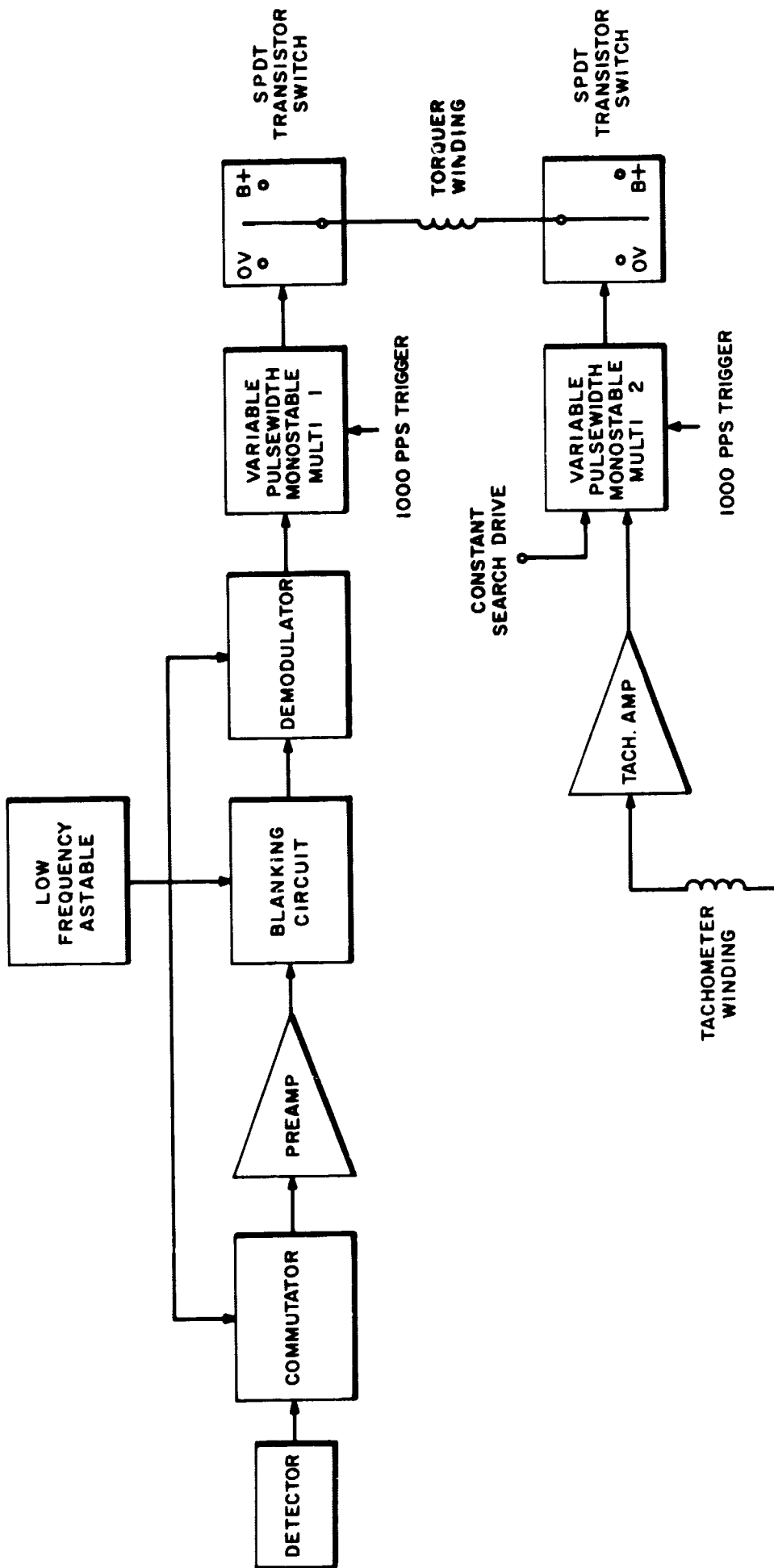
Figure 3-1   TORQUER DRIVE BLOCK DIAGRAM

21834

The on time of the first monostable multi will be controlled by the signal present in the main signal channel and will thus be proportional to the angular dip of the field of view of one thermopile below the horizon.

With no motion of the barrel, the on time of the second multi is constant and represents a search drive. Motion of the barrel generates a tachometer voltage, and thus will vary the on time around its "search value."

When both multivibrators are on or both multi-vibrators are off at the same time, both ends of the torquer winding are connected to equipotential points (both to ground or both to B+), thus producing no torque. Thus, in equilibrium, the search drive holds balance with the signal generated by the field of view dip.

To insure servo stability for a wide range of loop gains (radiant intensity variations of 30 or more), the tachometer amplifier is designed to provide a nonlinear gain characteristic (approximately exponential) with more than pro-portionally increasing damping for increasing velocities pointing from the planet edge toward space. For high system gains (400°K

moon edge), this will allow small amplitude limit cycles (dither) but no loss of track stability. This system has the advantage over a bang-bang servo of having considerably lower average power consumption. It has been breadboarded and tested on a laboratory model thermopile edge tracker at Barnes in February and it tracked stably on a "planet edge" whose temperature varies from 30°C to 230°C against a laboratory "space" of 25°C. With the optical passband between 14 and 18 microns used on this model, this corresponded to loop gain variations of more than 30 to 1. The total power consumption of the servo was about 100 milliwatts.

Circuit operation and design considerations for the variable pulse width monostable multivibrators, the exponential tachometer amplifier, and the single-pole, double-throw transistor power switches are given in Sections 3.1.1, 3.1.2, and 3.1.3 respectively.

3.1.1 Variable Pulse Width Monostable Multivibrators

The circuit is shown in Figure 3-2. In a conventional (fixed pulse width) monostable multivibrator, diode D1 would be absent. With no input pulse, Q1 is cut off, Q2 is
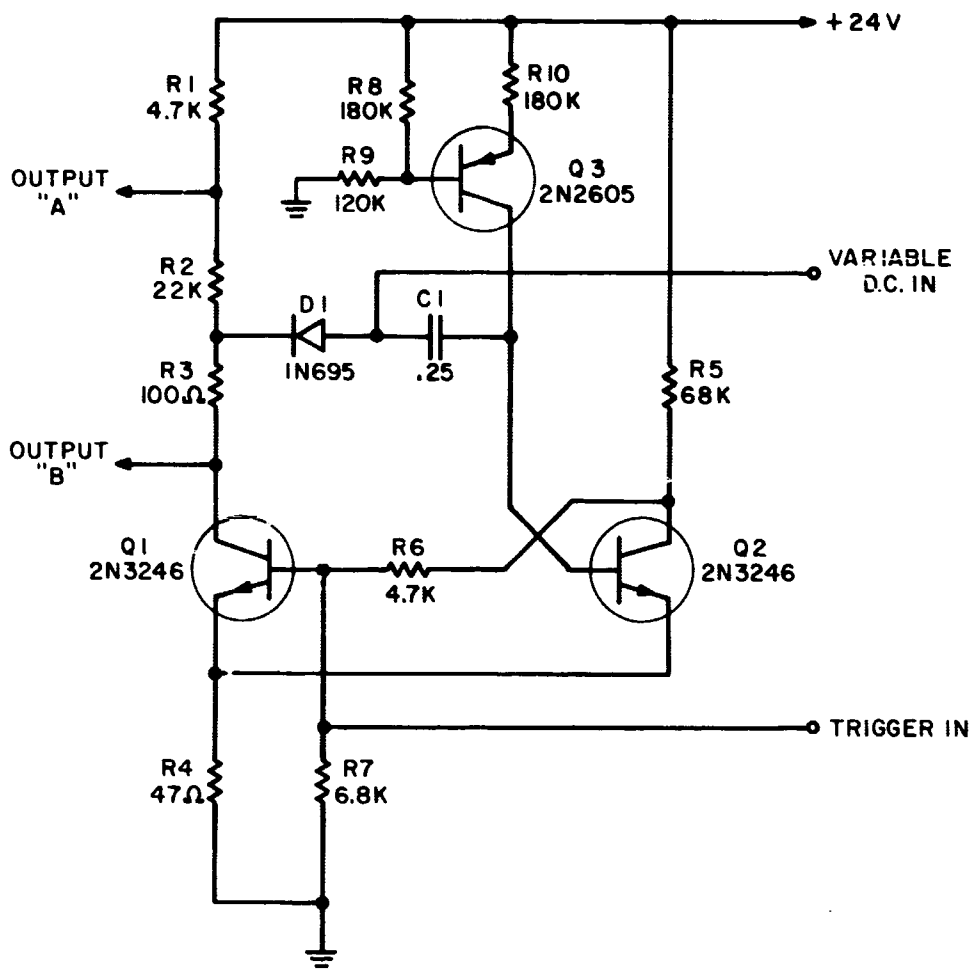
21835

Figure 3-2   VARIABLE PULSE-WIDTH MONOSTABLE MULTIVIBRATOR

conducting, and C1 is charged to the value of the d.c. supply voltage. When triggered, the pulse width of the multivibrator is determined by the time needed for C1 to discharge through the current source Q3. In the present circuit, D1 isolates C1 from the collector voltage of Q1 in the off state (steady state) of that transistor; and its charge (along with the time needed to discharge it, i.e., the pulse width of the multi) is determined by the external variable voltage fed to the junction of D1 and C1. The external voltage shall be derived from a source with an impedance low enough to permit recharging C1 before the next trigger pulse arrives and high enough to permit the collector of Q1 in its on state to drive C1.

The choice of points "A" and "B" at which the two outputs are taken is determined by the design of the single-pole, double-throw power switches described in Section 3.1.3.

3.1.2 Tachometer Amplifier

We conjectured that an exponential gain characteristic for the tachometer feedback would insure stability over a wide range of planetary intensities. This conjecture has been confirmed by experiment. Nevertheless, to prepare the

ground for a computer check on the system tolerances that will
still allow stable limit cycles, in the following the system
differential equations will be set up and the nonlinearities
specified.

The tracking operation is characterized by the block
diagram of Figure 3-3, a representation valid only if linearity
is assumed for all blocks. On the other hand, it provides a
ready way to write the system differential equation directly,
which in turn can be made to include the nonlinearities.

We can write for the overall <u>linear</u> transfer function

$$T(s) = \frac{(A_1 A_2 A_3)/(A_3 A_4 + 1)}{s(1 + s\tau_1)(1 + s\tau_2)(1 + s \frac{\tau_3}{A_3 A_4 + 1}) + A_1 A_2 A_3/(A_3 A_4 + 1)}$$
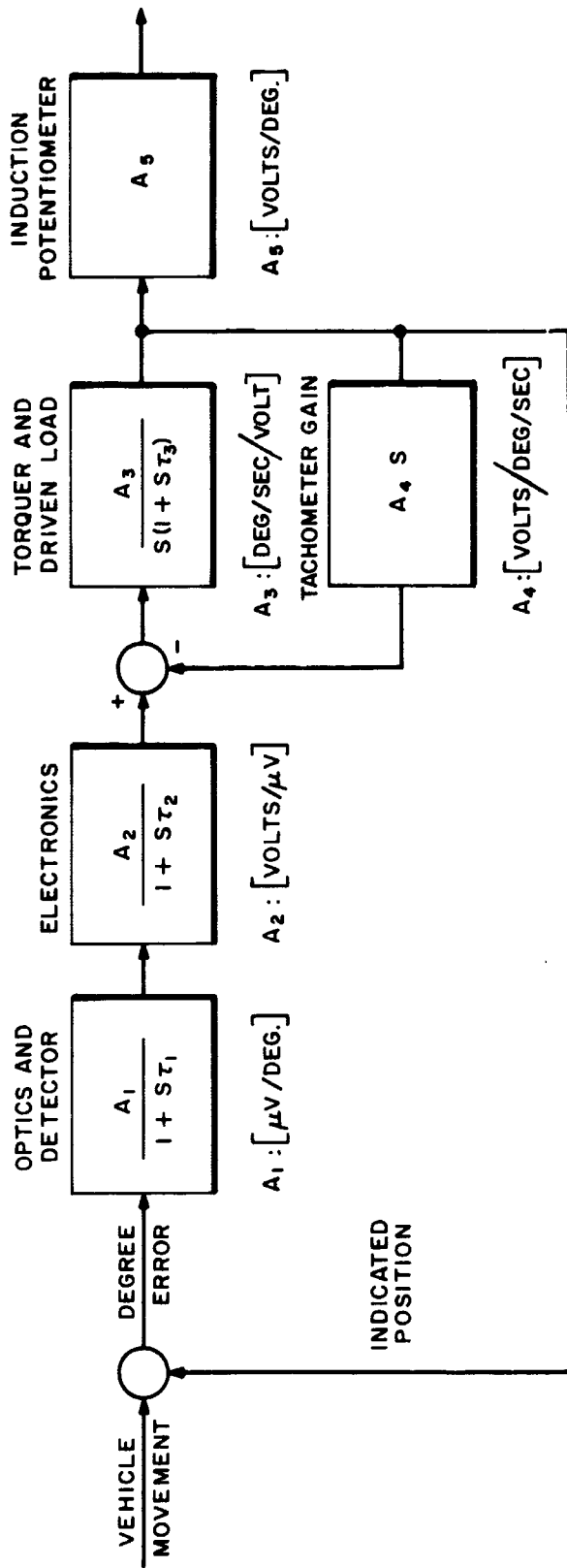
(Eq. 1)

a fourth order system. From here, the system differential
equation:

$$\theta'''' \frac{\tau_1 \tau_2 \tau_3}{A_3 A_4 + 1} + \theta''' (\tau_1 \tau_2 + (\tau_1 + \tau_2) \frac{\tau_1}{A_3 A_4 + 1})$$

$$+ \theta''(\tau_1 + \tau_2 + \frac{\tau_3}{A_3 A_4 + 1}) + \theta' + \theta \frac{A_1 A_2 A_3}{A_3 A_4 + 1} = 0$$

(Eq. 2)

Figure 3-3 LINEAR SYSTEM REPRESENTATION

21836

The nonlinearities of this equation are:

(1) In A_1 as a function of θ. This is due to system limitations (field of view of the thermopile in the direction θ). The nonlinearity is of the saturation type.

(2) A_2, the electronics gain, is also subject to saturation determined by the amplifier dynamic range. As A_1 and A_2 are represented in the equation jointly, as a product, the nonlinearity will be entered as such: a family of saturation characteristics $A_1A_2\theta$ versus θ with planet temperature as a running parameter (Figure 3-4).

(3) A_4, the tachometer gain, is made intentionally nonlinear (roughly exponential) with angular rates in order to insure tracking stability over all the $A_1A_2\theta$ characteristics represented in Figure 3-4. The desired characteristic $A_4\theta'$ versus θ' is shown in Figure 3-5, and A_4 is the slope of this characteristic.

The computer solution would proceed by initially neglecting the terms with the third and fourth order derivatives and would get a rough evaluation of the stability by a phase-plane analysis of the remaining second-order equation
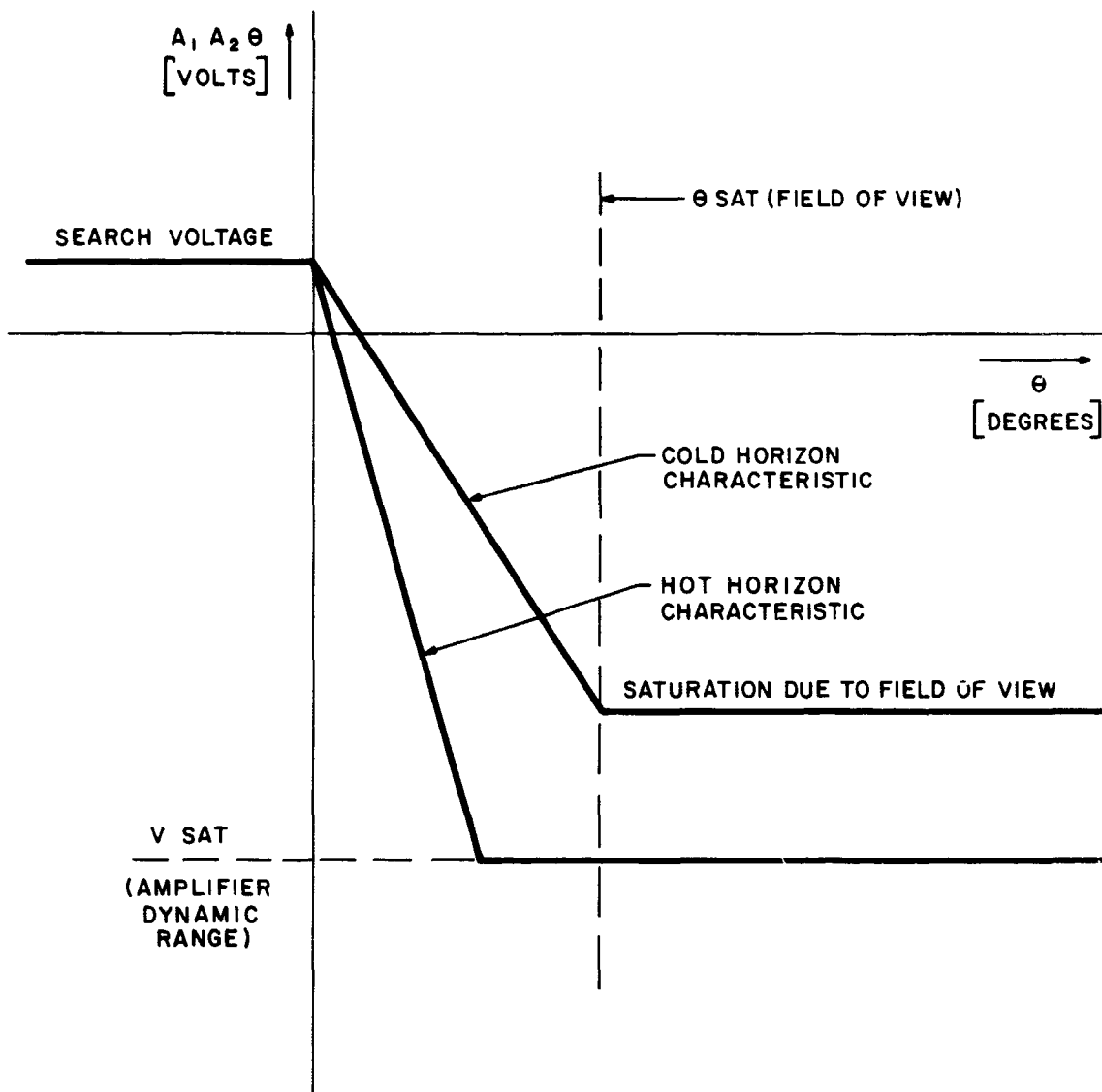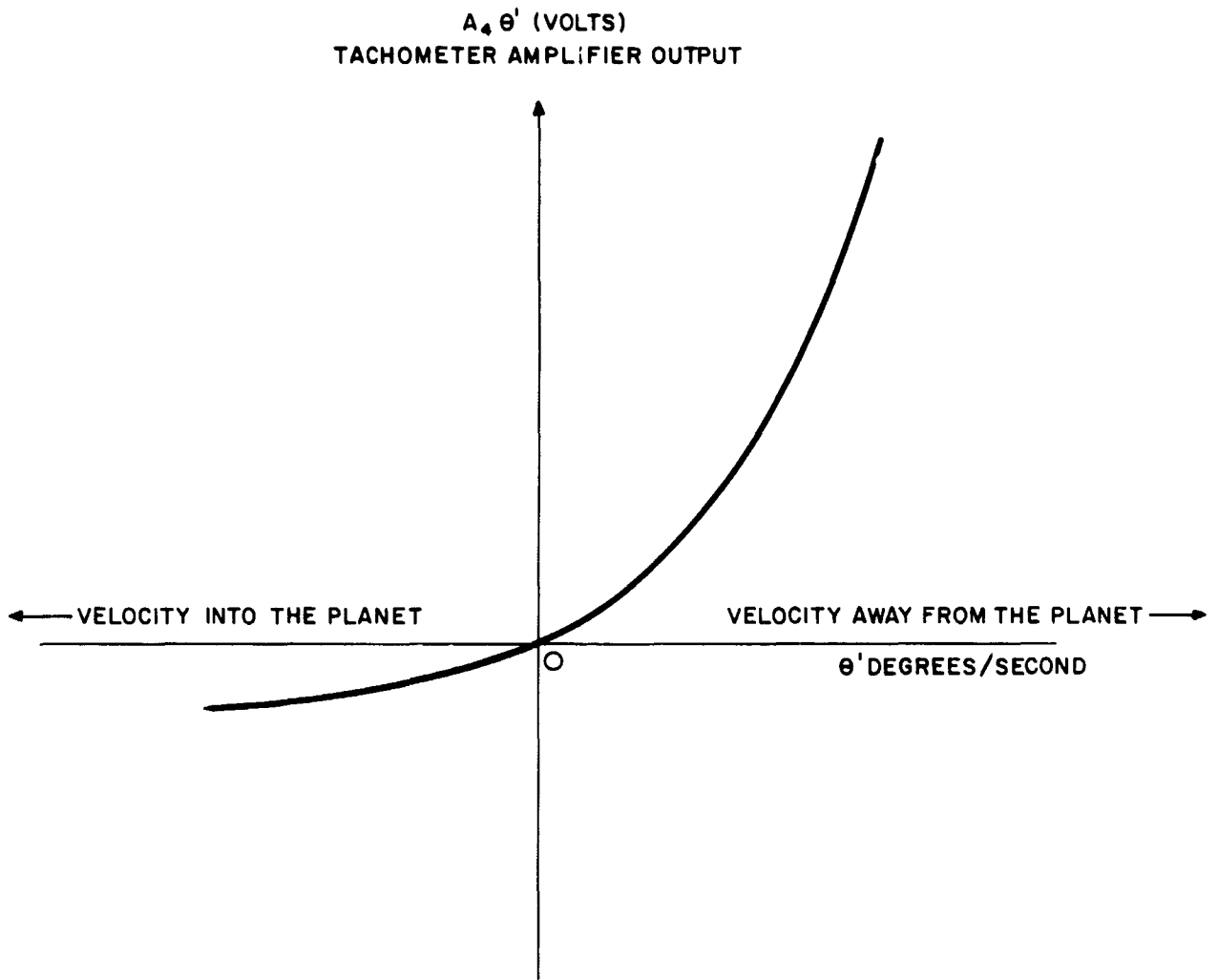
Figure 3-4 SATURATION OF A₁ A₂ Θ

A₄ θ' (VOLTS)
TACHOMETER AMPLIFIER OUTPUT

←——— VELOCITY INTO THE PLANET

VELOCITY AWAY FROM THE PLANET ——→

O

θ' DEGREES/SECOND

21838

Figure 3-5   TACHOMETER FEEDBACK CHARACTERISTIC

with its intentional and nonintentional nonlinearities. Then, considering rates and accelerations <u>along</u> the calculated limit cycles, by successive approximations, the stability of the fourth order equation could be determined.

The $A_4\theta'$ characteristic of Figure 3-5 has been synthesized by driving a common emitter transistor amplifier, biased to the turning on point of the base-emitter junction, from the low impedance of the tachometer winding (Figure 3-6). Diode D1 provides the proper bias voltage and the exponential characteristic is realized by the I_c versus V_{be} curve of Q1. D1 also provides an ambient temperature stabilization of the circuit. D2 temperature compensates the base-emitter junction of emitter follower Q2.

3.1.3 Power Switches

Figure 3-7 is a circuit diagram of the torquer drive circuit. The two ends of the torquer winding are handled in a symmetrical manner. Either end is connected to or disconnected from the positive supply by means of a medium power PNP transistor. The connection/disconnection to or from ground is done by means of an NPN transistor. Each of these is driven
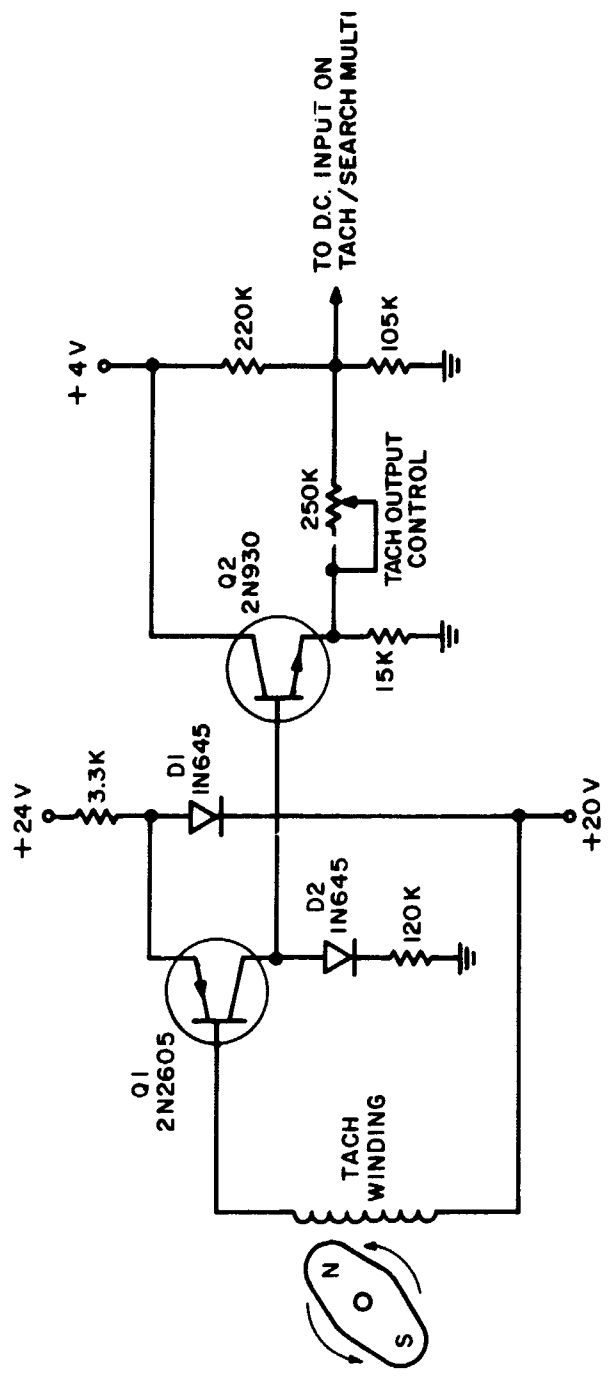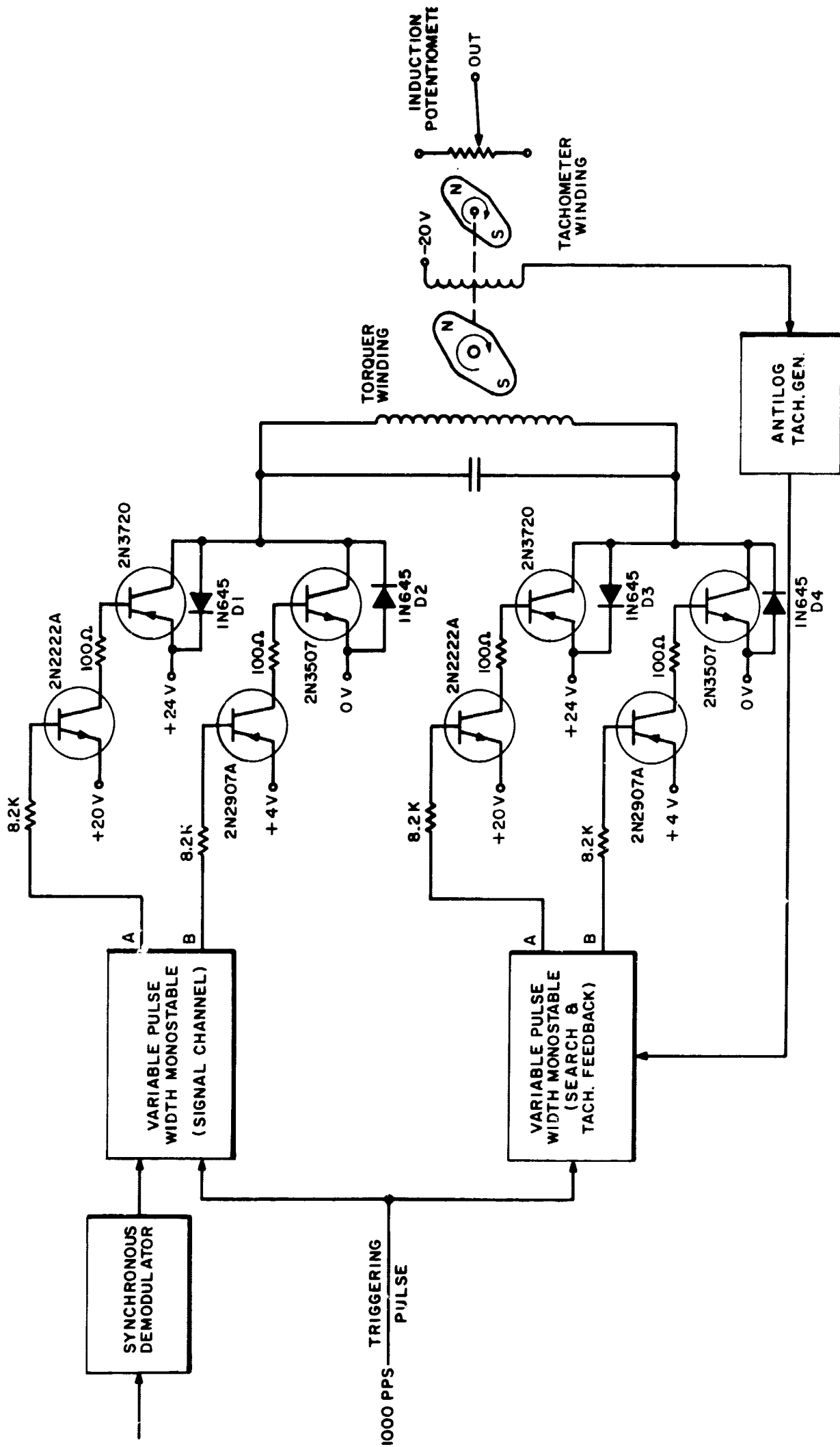
Figure 3-6   ANTILOG TACH GENERATOR

21839

Figure 3-7   MOTOR DRIVE CIRCUITRY

21840

by means of a low power transistor, driven in turn by outputs "A" or "B" of one of the variable pulse width monostable multi-vibrators. Resistors R_1, R_2, and R_3 in Figure 3-7 are chosen so as to provide the proper turning on and turning off voltages to these low power drivers.

The selection of the power transistors represents a good compromise between size, power handling capability, current gain, and collector-to-emitter saturation voltage. The current gain will primarily determine the in-track power requirements by setting a lower limit on the turning-on base current which is needed where the collector, and thus the torquer, is passing current or not. This base current will be derived from a low voltage output of the instrument power supply in order to reduce the power losses connected with this current consumption. This explains the presence of the terminals marked +20V and +4V in the diagram of Figure 3-7. The availability of these voltages also facilitates the design of the tachometer amplifier.

The saturation voltage of the power transistors determines their power dissipation in the search mode and during transients in tracking.

Diodes D1 through D4 serve to short out the inductive transient voltage of the torquer winding upon switching off the torquer current and thus eliminate this contribution to transistor power dissipation.

3.2 Front End of the Signal Channel

A MOS FET commutator feeds the output of the two thermopiles to the preamplifier. The output of the preamplifier is freed from the commutation spikes by means of a blanking circuit driven in synchronism with the commutator (Figure 3-8). The MOS FET circuitry has been proven in several instruments designed at Barnes Engineering Company, and a 90-element commutator has been operating without any failures in an all-solid-state horizon sensor designed and delivered to the Jet Propulsion Laboratory of the California Institute of Technology. In the breadboard tests, a 70 cps commutation drive was used.

The preamplifier used in the breadboard tests is represented in Figure 3-9. It is a flatpack microcircuit amplifier driven by a low-noise, first-stage discrete transistor. Tests still continue to select the microcircuit amplifier most appropriate for our use.
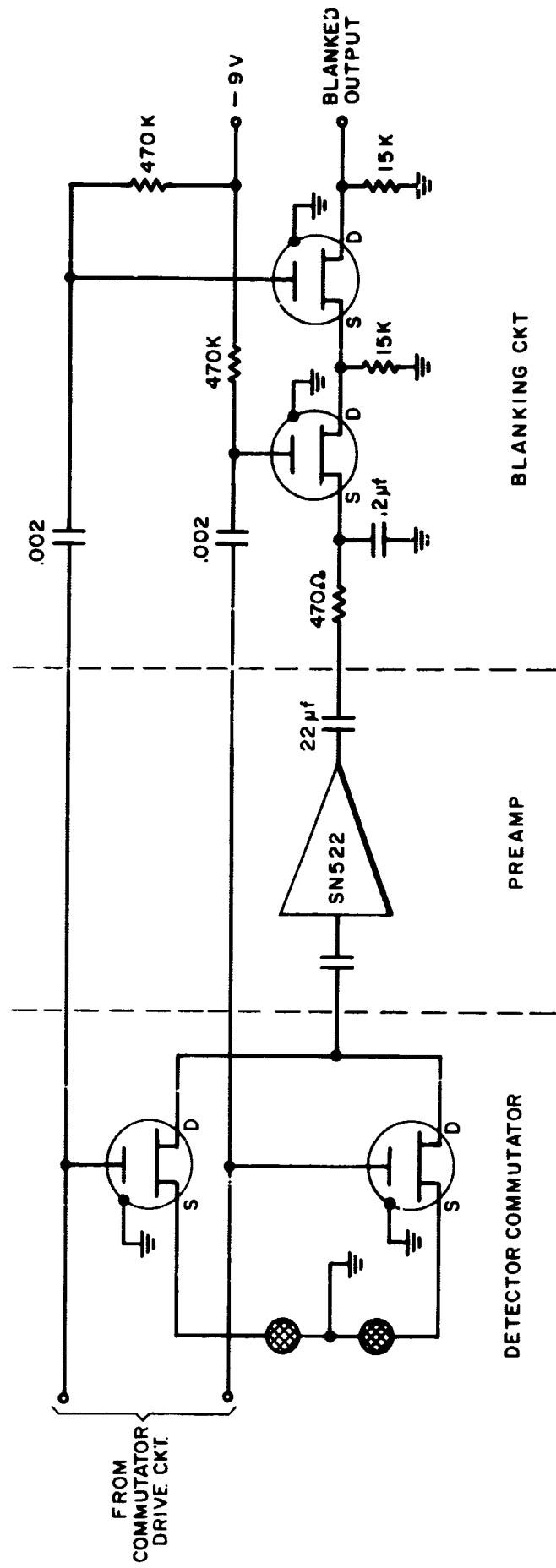
Figure 3-8   SIGNEL CHANNEL FRONT END
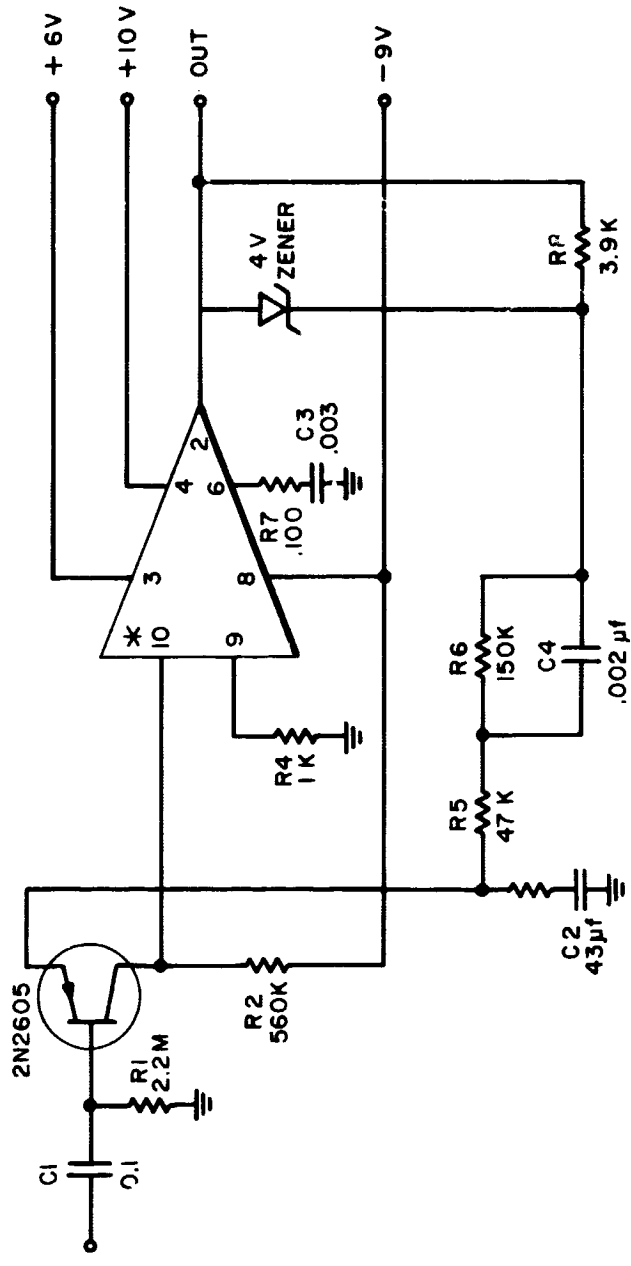
* TEXAS INSTRUMENT SN522
MICROELECTRONIC OPERATIONAL AMPLIFIER

Figure 3-9   PREAMPLIFIER

4. CALCULATION OF HORIZON SENSOR SYSTEM SENSITIVITY

As outlined in the foregoing sections, the system will have a 2-inch diameter optical collector and will use thermopile detectors which will view fields of view of 1.5° width and 10° in length. With these parameters established, we can calculate the system sensitivity which we expect to achieve.

We will first consider the worst case, that of a 90°K lunar temperature. This is believed to be ultra conservative, since the bulk of evidence indicates higher temperatures and since the 10° length of the field of view will provide some integration over the surface of the moon's edge, including the possible cool craters as well as high surfaces with greater exposure to solar radiation and which will thus be warmer.

The radiance from a 90°K blackbody is about 10^{-4} and 60% of this lies in the spectral region from 14 to 40 microns. We will therefore assume a radiance:

$$\Delta N_{\lambda 90°K} = 6 \times 10^{-5} \text{ watts/cm}^2\text{-steradian}$$

Had we taken the lunar temperature to be 110°K--a more likely figure--the radiance would be approximately twice this value.

The power on the detector for the optical collecting system is given by:

$$P_D = \Delta N \, A_o \, \omega \, \epsilon$$

where

A_o = optical collecting area

ϵ = optical efficiency

ω = solid angle or field of view in radians squared

For an angle of α radians, then $\omega = \alpha^2$.
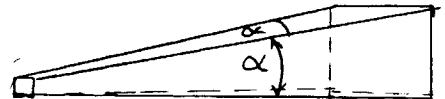
For circular optics, we may write:

$$P_D = \frac{\pi}{4} (\sin\alpha)^2 \, \Delta N \, A_o \, \epsilon$$

For small angles, $\alpha \approx \sin\alpha$, where θ is in radians.
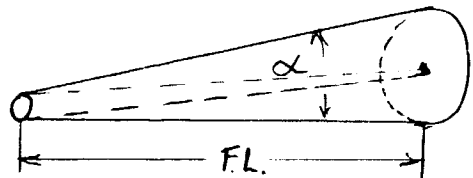
The detector length is given by: $L = (FL \sin \alpha) \approx (FL \, \alpha)$ for small angles, where FL denotes the focal length.

The detector area, $A_d = (FL)^2 \, \omega$.

The f/number of the system:

$$f/no. = \frac{\text{focal length}}{\text{diameter of optic}} = \frac{FL}{D}$$

We can express the power on a detector of specific

area as:

$$\frac{P_D}{A_d} = \frac{\pi}{4} \frac{D^2 \Delta N \ \epsilon}{(FL)^2} \qquad \text{since } f/no. = FL/D$$

We can write this as:

$$\frac{P_D}{A_d} = \frac{\pi}{4} \frac{\Delta N \ \epsilon}{(f/no.)^2}$$

For a thermopile detector, the specific responsivity:

$$\mathcal{R}' = \frac{V_D}{P_D/A_d}$$

Therefore, the signal developed by the detector:

$$V_D = \frac{\pi}{4} \frac{\Delta N \ \epsilon \ \mathcal{R}'}{(f/no.)^2}$$

where

ϵ = the efficiency of the optics = 0.3

$\mathcal{R}'$ = specific responsivity of the thermopile = 1.7 V/w/cm^2
for an array of 50 junctions of bismuth-tellurium

f/no. = f/number of the optics--we have chosen an f/1 system

(Note the dependence of output signal on the
f/number which will be referred to later on.)

$$V_D = \frac{\pi}{4} \frac{6 \times 10^{-5} \times 0.3 \times 1.7}{1^2} = 24 \text{ microvolts}$$

This is the signal which would be received if the entire detector were illuminated. Since the detector width is 1.5° and we wish to arrange the sensor to track the edge when the detector indentation is only 0.2° (to achieve a 0.1° accuracy), the signal for this amount of indentation will be (0.2/1.5) x 24 microvolts. $V_D/0.20 = 3.2$ microvolts. A 110°K lunar edge will result in twice this signal.

The detector which we plan to use has 50 pairs of thermocouple junctions (active and compensating) and will have a resistance, R_d, of about 50,000 ohms. Noise of this detector will be principally Johnson noise. At the synchronous demodulator output we will obtain a small amount of this noise within the filter passband, Δf, of the output and centered at the demodulator carrier frequency. In a one-cycle output bandwidth, the noise referred to the input of the system will be:

$$V_J = \sqrt{4KTR_d\Delta f} \simeq 0.03 \text{ microvolts rms}$$

This is clearly far lower than the signals expected and can be considered negligible.

More significant will be any small d.c. voltages at the modulator input which are due to thermal emf's arising from possible temperature differences at wiring connections between the thermopile and the modulator (inadvertent thermocouples). Using our present technology in the thermal design of the input components and the choice of materials for the wires and solder, we have been able to control such undesired thermal voltages or drifts to about ±0.5 microvolts over the range of ambient temperatures of -10°C to +60°C. We will therefore use this ±0.5 microvolt drift as the fundamental limitation for our system.

The signal-to-noise ratio (or drift) for a total 90°K lunar edge region would therefore be 3.2/0.5 = 6.4, and is more likely to be twice this amount when integrated over a 10° lunar edge, even for the coldest portion of the moon.

In an orbit around the earth, the sensor will be dealing with higher temperature regions at the horizon. In the 14 to 20 micron region, the lowest temperature in the region

of the limb will be about 200°K. This gives rise to a radiance
of 7.8 x 10^{-3} watts/cm^2-steradian, of which about 70% is in the
14 to 40 micron range, which our silicon optics will transmit.
Thus

$$\Delta N_{200°K} \; 14\text{-}40\mu = 2 \times 10^{-3} \text{ watts/cm}^2\text{-ster}$$

or about 30 times the energy from the edge of the cold side of
the moon. This would give rise to a signal level of about 104
microvolts and signal-to-drift ratio of 208. It will therefore
be very easy to achieve a high tracking accuracy with this
system, particularly in an earth orbit. The threshold level
for the system, which will establish the point at which the
horizon will be tracked, will be set far below this signal
level (in fact, in the vicinity of 3 microvolts). Consequently,
we will be tracking a region in the upper atmosphere where the
radiance levels for various geographic and seasonal conditions
to be encountered are quite uniform (see Figure 2-1 of the
Phase IA Study Report) and the angular error can be made quite
small.

It is interesting to note that the choice of optical
speed in the design of this horizon sensor system is not critical

in the least, despite the fact that the term $f/no.^2$ appears

in the denominator of the expression for detector signal V_D

referred to earlier.   Instead, optical collector area becomes

a significant factor which could be increased to achieve a

direct increase in signal-to-noise (drift) ratio.

The reason for the lack of dependence on optical

speed is to be found in the fact that, other things being

equal (collector area and optical transmission), a faster

optical speed requires use of a smaller detector with conse-

quent reduction in the number of series-connected, voltage-

generating junctions. Also, for a given detector field of

view width, since we can only tolerate a 0.2° indentation

(penetration) of the planet edge, the greater detector width

of a short focal length system is a detriment to the S/N ratio.

This is illustrated in the table following, which compares the

performance of systems with various optical speeds. The tabu-

lation assumes a 2-inch diameter optical collector and a 10°

field of view length--the detector width and element density

being held constant. (The threshold level is assumed to be

limited by thermal drifts and not resistance noise as explained

earlier.) A radiance for earth application of 2×10^{-3} watts/

cm^2-steradian is assumed.

TABLE 4-1   Comparison of Systems with Various Optical Speeds

F/No.	Field of View Length	Width	Detector Size Length	Width	Number of Junctions	Responsivity $v/w/cm^2$	Signal for Full Detector Illumination	Signal (V_D) for 2° Indentation
f/2	10°	0.77°	17 mm	1.3 mm	98	3.4	400 μv	104 μv
f/1	10°	1.54°	8.5 mm	1.3 mm	49	1.7	800 μv	104 μv
f/0.5	10°	3°	4.25 mm	1.3 mm	24	0.85	1600 μv	104 μv

APPENDIX A

Special Technical Report
Earth/Lunar Horizon Sensor System

"Recommendation of Thermopile Detectors for Field
Switched Edge Tracking Horizon Sensor"

In the course of design effort toward the Earth/Lunar Horizon
Sensor using a field switching edge tracker approach, certain
factors which were not fully resolved in the trade-off study
phase of the program have been brought into sharper focus.
These pertain specifically to the optical design parameters
to effect a wide separation of the two switched fields of view.
In recent discussions with NASA personnel, we recognized the
need to separate the two fields of view by a large enough amount
to avoid any possibility of both fields of view being pointed
on the surface of the planet at the time the sensor is turned
on. Such a condition could conceivably result in tracking of
the terminator or other temperature gradient.

Barnes Engineering Company is in full agreement with the desir-
ability of increasing the separation of the two fields. How-
ever, in attempting to accomplish this objective, certain
difficulties were encountered: An attempt to recombine the
separated fields onto a reasonably small detector requires an
optical system which is critical and complex. An alternative
is to use a larger detector and accept a reduction in avail-
able signal-to-noise ratio.

In the light of these new difficulties, we reviewed the results of the trade-off and it appears that under these conditions the thermopile version of the field switched edge tracker offers definite advantages.

As will be briefly shown below, the deviation in detector choice will result in a number of advantages in terms of reliability, power, weight, and successful rapid execution of the program in the limited time available to the due date for the engineering model. First, I wish to describe the edge tracking horizon sensor as we presently envision it. Next, I will compare the various performance characteristics for the field switched edge tracker as designed with thermistor and thermopile detectors. In this discussion, I will indicate the differences and compromises which must be made in the final system design, and with it, the reason for the departure from the original detector choice.

A. The optical/mechanical system and block diagrams are seen in Figures 1 and 2.

Two thermopile detectors subtending 1° x 10° are located in the focal plane of the objective. Their separation is made to correspond to the desired field switched displacement angle (12°, as shown in Figure 2). The optical barrel is rotated by the brushless torquer to track the horizon edge. The objective we chose is a 2-1/2 inch diameter silicon lens. Signal to noise will vary approximately linearly with collector area. (It will be recalled that in the case of the thermistor version, because of the undesirability of moving the vibrating optical chopper, a plane mirror was placed in front of the objective and rotated by the torquer. For a 2-inch objective, the plane mirror has to be 4 inches long.)

B. A comparison of characteristics of the field switched edge tracker using thermopile and thermistor detectors is shown in the attached chart. Since the worst case to be considered is that of use on the cold side of the moon, only the signal-to-noise ratio for the case of a 90°K target will be considered (spectral passband of 14-40 microns assumed). In the case of earth orbit applications, the signal-to-noise ratio will, of course, be far better. It is also to be expected

that lunar surface temperatures will be higher than the 90°K
assumed value, particularly in view of the fact that the energy
will be integrated in the case of the thermopile sensor over
a strip 10° in length.

C. As the optical design for the thermistor approach pro-
gressed, it became evident that a penalty had to be paid in
terms of sensitivity, for increased separation of the two
fields of view. The detector size had to be increased, re-
sulting in poorer detector sensitivity (and larger bias voltage)
In addition, due to the rectangular detector configuration, an
immersion lens design would yield optimum optical speed (f/0.2)
in only one dimension of the field of view. Further, absorption
losses in the hyperimmersion lens would result in some signal
losses.

The attached chart shows a relative improvement of the
thermopile detector under the specific conditions chosen.
The following considerations account for the similarity of
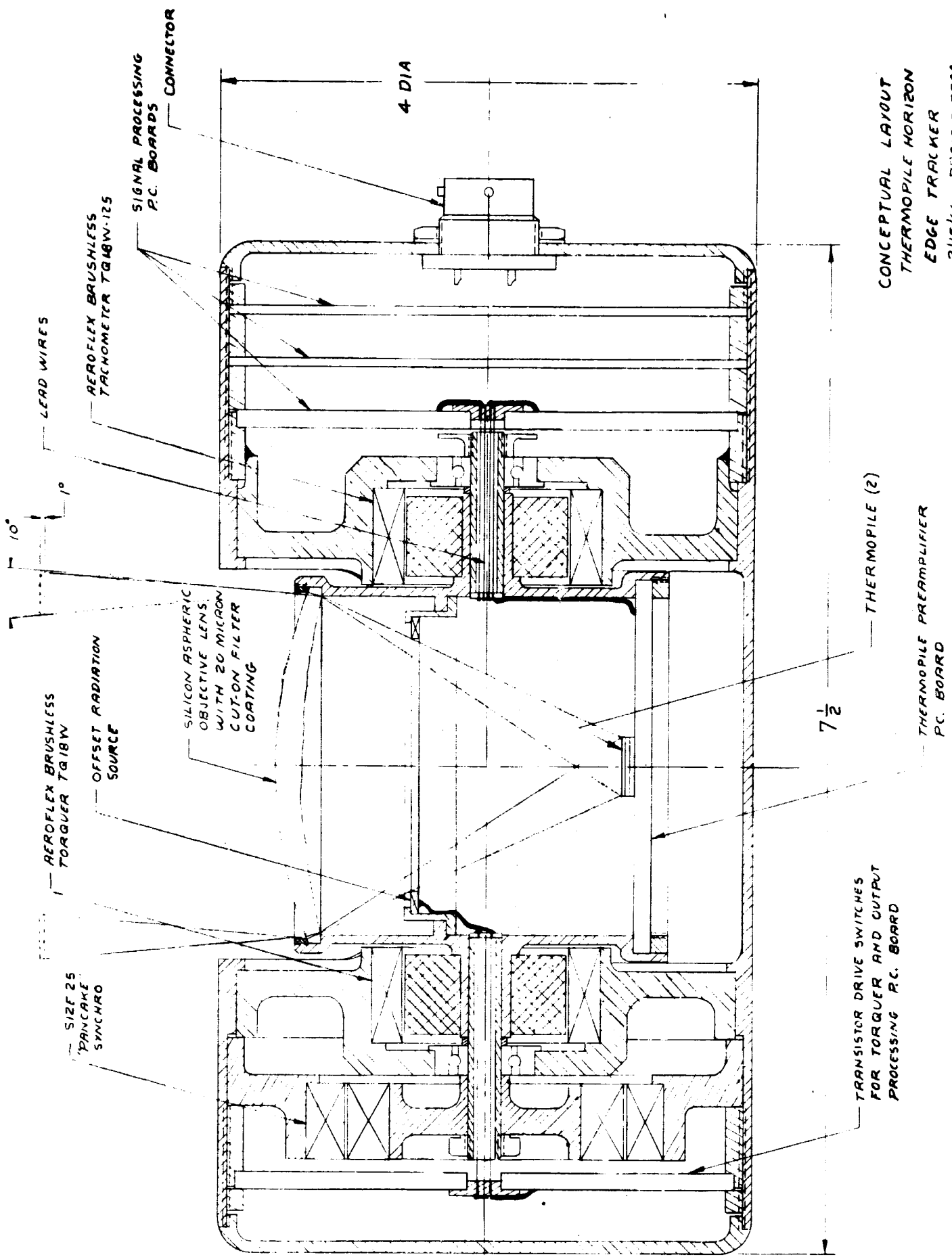signal-to-noise ratios for the two detector types:

(1) A larger objective can be used with the thermo-
     pile system (2-1/2 inches versus 2 inches) while
     resulting in an overall size and weight reduction,
     since this system eliminates the need for a 4-
     inch plane mirror. The net advantage is a 1 5X
     signal increase.

(2) Field of view of the thermopile system is con-
     veniently made twice that of the thermistor
     This is because the sensitivity of the thermo-
     pile improves with larger areas (more junctions)
     while that of thermistors is degraded. The im-
     provement of the thermopile is 2X on the basis
     of the larger field of view.

(3) Responsivity of the thermopile in vacuum is
     improved by a factor of more than two, as
     recently measured. This factor was not consid-
     ered in our earlier calculations. Our sensitivity
     figures are based on use of bismuth-tellurium
     detectors which yield the highest responsivity we
     have been able to achieve.

(4) Responsivity of the thermistor is degraded for the larger detector by a factor of about two as imposed by the larger separation of the fields

(5) The absorption and reflection losses when the immersion lens is considered account for a factor of two loss in efficiency for the thermistor detector.

Combining these factors, we account for a total of 20. Under ideal conditions, the optimum hyperimmersed thermistor is better than the thermopile by about this factor. In the present realistic system, the signal-to-noise ratios of the two detectors considered are about equal and other considerations tend to favor the thermopile.

Summarizing the above remarks, we find that the thermopile detector has about the same signal-to-noise ratio in the present application as the immersed thermistor. In other respects the use of this detector results in various powerful advantages. Eliminating the vibrating optical chopper with some associated electronic simplifications results in a significant improvement and simplification of the optics. It also permits a wider search angle, if desired, and readily changeable field of view separation angles. In addition, this provides for a reduction in size, weight, and power, as well as an improvement in reliability. All these advantages and the greater flexibility in using this detector approach compel us to recommend use of the thermopile detector in the present application.

We feel confident that the approach outlined above can be successfully transformed into the engineering model specified by our contract and that the work can be completed on the present schedule. In part, this confidence is based on the experience with an elementary breadboard version of such a sensor which has been built and tested on an independent Company-sponsored program. We will be glad to demonstrate operation of this unit to interested NASA/MSC personnel

CONNECTOR

SIGNAL PROCESSING
P.C. BOARDS

AEROFLEX BRUSHLESS
TACHOMETER TG18W-125

LEAD WIRES

10°   1°

AEROFLEX BRUSHLESS
TORQUER TG18W

OFFSET RADIATION
SOURCE

SILICON ASPHERIC
OBJECTIVE LENS
WITH 20 MICRON
CUT-ON FILTER
COATING

SIZE 25
"PANCAKE"
SYNCHRO

4 DIA

THERMOPILE (2)

THERMOPILE PREAMPLIFIER
P.C. BOARD

$7\frac{1}{2}$

TRANSISTOR DRIVE SWITCHES
FOR TORQUER AND OUTPUT
PROCESSING P.C. BOARD

CONCEPTUAL LAYOUT
THERMOPILE HORIZON
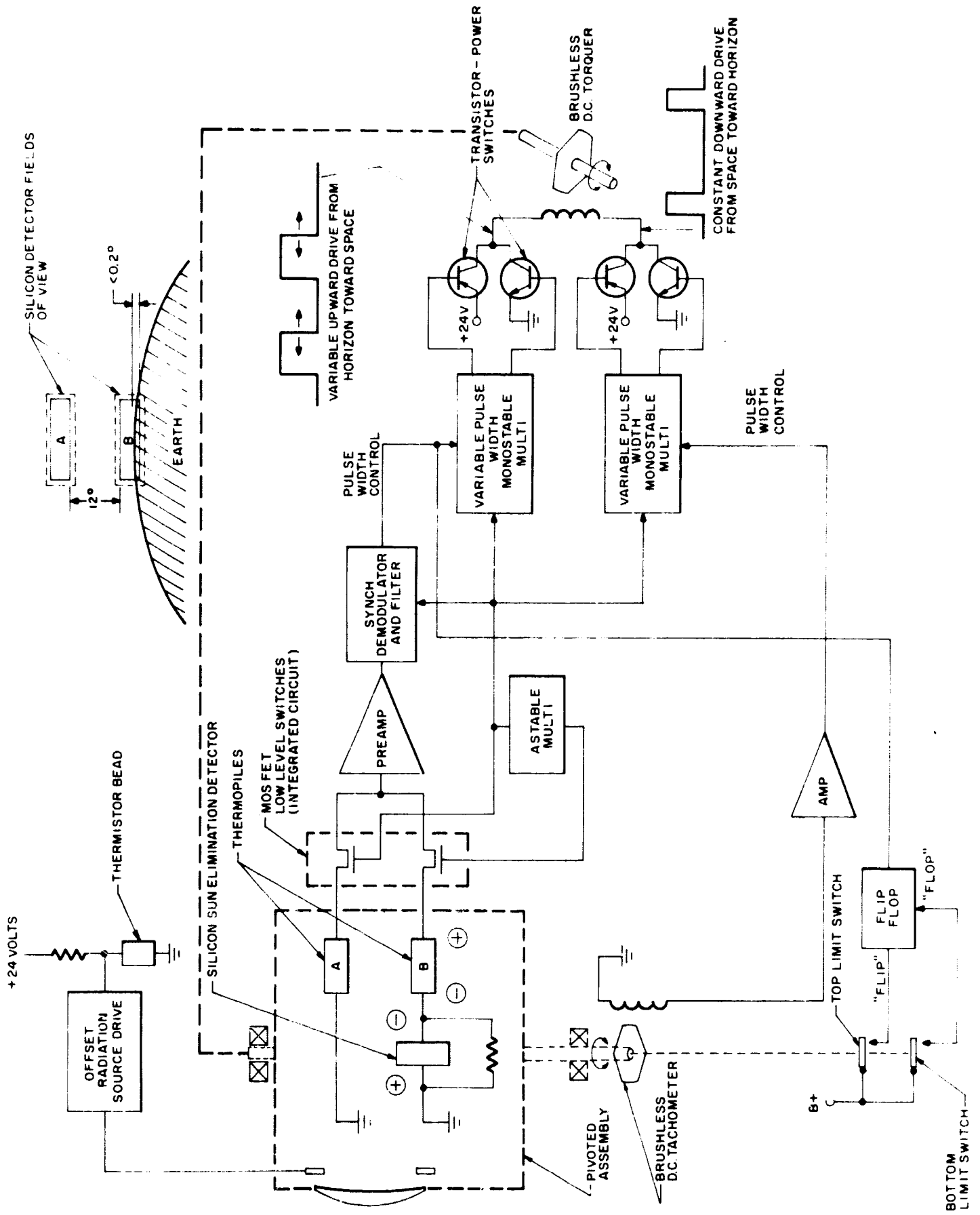EDGE TRACKER
2/15/66   PROJECT 3744

Figure 2 BLOCK DIAGRAM OF ONE HEAD THERMOPILE HORIZON EDGE TRACKER
(THREE HEADS REQUIRED FOR TWO-AXIS OPERATION)

TABLE I. COMPARISON OF FIELD SWITCHED EDGE

CHARACTERISTIC	THERMOPILE
Aperture	2-1/2" Si l tracking fu
System Field of View	$1^\circ \times 10^\circ$
Field Separation	12° readily
Optical Speed	f/1
Detector Size	1.1 mm x 11
Sensitivity	$V_D = \frac{\pi}{4} \frac{\Delta N}{f}$ $V_n = \, < 1\mu$
S/N for 0.2° Indentation	$\frac{S}{N} = 10$ for (
Expected Instrument Accuracy	$\pm 0.1^\circ$
Reliability	50% higher
Power Comparison	Approx. 5 W
Weight	$\simeq$ 10 lbs
Temperature Range	Stable over
Comments	Improvement made contin the performa much simple
Schedule & Cost to Completion	We believe goals with

	THERMISTOR
ns with associated detector performs ction	2" Sl lens - a 4" plane mirror required for track mode
	$1^\circ \times 6^\circ$
changed to other values	6.6°
	f/.2 for narrow dimension only
mm $R^1 = 2.1V/w$	2 mm $\times$ 1 mm $\Delta N/_{90^\circ K} = 6 \times 10^{-5}$ $A_o = 20$ cm^2 $\xi = .25$ $\omega = .2^\circ \times 6^\circ$
$R^1 \simeq 50\mu V$	$P_D/._2 o = \Delta N \omega A_o \xi = 10^{-7}$
V over temperature range	eff NEP = 10^{-8} Watts based on p-p noise
$.2^\circ$ Indentation on all $-90^\circ K$ target area	S/N = 10
	$\pm 0.1^\circ$
ITBF	
tts	About 25% higher
or three heads	About 30% higher
range of $-50^\circ C$ to $+ 100^\circ C$	Restricted to $-20^\circ C$ to $+60^\circ C$ with responsivity variations in this range
in sensitivity of thermopiles are being iously and are expected to further improve ince of this system. Optical design is	
t will be possible to meet the design his system on schedule.	Complexity of optical & mechanical design may result in a delay both in the detail design study report & system completion.